Turk J Chem
30 (2006) , 1 – 13.

Analysis of Nanoparticle Transmission Electron Microscopy Data Using a Public- Domain Image-Processing Program, *Image*

Gerd H. WOEHRLE[1], James E. HUTCHISON[1*], Saim ÖZKAR[2*], Richard G. FINKE[3*]

[1] *Department of Chemistry and the Materials Science Institute, University of Oregon, Eugene, OR 97403-1253 USA*

[2] *Department of Chemistry, Middle East Technical University, 06531 Ankara-TURKEY*

[3] *Department of Chemistry, Colorado State University, Fort Collins, CO 80523 USA*

Received 02.08.2005

The need to easily and quickly count larger numbers of nanoparticles, in order to obtain statistically useful size and size-distribution data, is addressed via the use of a readily available, free, public-domain program for particle counting, NIH-*Image* (and 2 others derived from it, Scion Image and Image J), collectively referred to herein as *Image*. The best protocols that we have found useful for the use of *Image* are reported; both appropriate as well as problematic applications of *Image* are then illustrated with a series of TEM images of Ir(0), Pd(0) and Au(0) nanoclusters. Methods to detect and image nanoclusters with sub-1-nm core diameters are reported and illustrated in the literature with Au nanoclusters, an important problem since the literature indicates that subnanometer Au nanoclusters are often present, but undetected. A list of suggestions and caveats for the appropriate use of *Image* is also provided, since this contribution is directed at first-time users who are not presently using nanoparticle imaging software. The reader is also reminded of several, well-known caveats for the use of TEM in obtaining size data for nanostructures. Overall, *Image* is a free, public-domain program that is useful for the rapid counting of large numbers of particles.

Key Words: Nanoparticles, Particle size distributions, Transmission Electron Microscopy, Image analysis, *Image* (NIH-Image, Scion Image, Image J), Histograms.

Introduction

Nanoparticles—that is, particles with core diameters of 1-100 nm possessing unique chemical and physical properties arising from their nanoscale dimensions[1−4]—continue to be of significant current interest for their potential applications in catalysis[5], quantum computers[6], optical, electronic, or magnetic devices[7], chemical

*Corresponding author

sensors[8], ferrofluids for cell separations[9], as components in industrial lithography[10] or in photochemical devices such as flat-panel displays[11]. In each of these applications the size and size distribution of the nanoparticles are a primary concern.

Transmission electron microscopy (TEM) is almost always the first method used to determine the size and size distribution of nanoparticle samples[12]. Once a representative group of images is obtained[13], the next task is to count as many particles as possible, ideally a few thousand, so that good statistics on the size and size distribution present can be obtained. This counting step is where the "by eye and by hand" method, still common in the literature, has problems: such methods are tedious, often result in a few hundred or fewer particles being counted, and hence yield poor statistics despite all one's effort. In addition, this procedure is inherently open to human errors and subjectivity.

For the above reasons, computer image processing methods are of interest for counting a relatively large number of particles, with as much objectivity in the process as possible. This image processing need is recognized in a report on commercial software for nanoparticle counting[14]. There are also earlier papers on computer-assisted counting of nanoparticle images[15] and automated image analysis based on a deformable ellipse model[16]. Other commercial software packages exist and have been used for this purpose, such as SPIP (Image Metrology ApS)[17], LUCIA (Laboratory Imaging)[18] and KONTRON KS 400 (Zeiss-Kontron)[19,20].

Herein we report on the use of a readily available, free, public domain program that we and others[21] have found useful for the rapid counting of nanoparticles, NIH-*Image.* This program, and 2 others derived from it, Scion Image and Image J, will collectively be referred to hereafter as *Image* except where the need arises to mention specifically an individual program. *Image* is useful, easy and fast. Image is not mentioned[22] in either of the prior 2 papers on computer imaging of nanoparticles[15]MACS:1997. Hence, we report our results to date using *Image* as a service to the community. Also reported herein is our use of *Image*, when coupled with appropriate sample preparation and TEM analysis methods, to detect and count Au nanoparticles with sub-1-nm core diameters, thereby addressing the current problem in the Au nanoparticle literature of missed sub-nanometer particles[23,24].

Experimental

Obtaining Image. Versions of these public domain programs, NIH-Image or Scion Image for Macintosh computers, Scion Image for Windows, and Image J, the Java-based version that runs on Linux, Mac OS 9, Mac OS X and Windows, are available at

http://rsb.info.nih.gov/nih-image/index.html,

http://www.scioncorp.com/pages/scion_image_mac.htm,

http://www.scioncorp.com/pages/scion_image_windows.htm and

http://rsb.info.nih.gov/ij/, respectively.

TEM Sample Preparation. Appropriate sample preparation to obtain well-dispersed, isolated particles is a well-recognized, crucial step in the TEM analysis process[12,13]. The solutions used for the TEM experiments were prepared as described in our earlier papers[21a−d,25,26]. Briefly, iridium nanoclusters were obtained from the Standard Conditions[27] hydrogenation of 1.6 M cyclohexene starting with 1.2 mM of the nanocluster precursor complex (a (1,5-COD)Ir^+ complex) and 1.2 mM stabilizer in acetone at 22.0 ± 0.1 °C. After the completion of the nanocluster formation (monitored by GLC determination of cyclooctane

evolved from the reduction of the (1,5-COD)Ir^+ precursor complex), the Fischer-Porter (F-P) bottle was detached from the hydrogenation line via its quick-connects, brought back into an inert (N_2) atmosphere drybox, and its acetone solution was quantitatively transferred with a disposable polyethylene pipette into a clean, 5 mL screw-capped glass vial. The solution was dried under vacuum and the glass vial was then sealed and brought out of the drybox. The dry nanocluster samples in screw-capped glass vials were sent as solids to the University of Oregon, where the TEM images were obtained. There, 1 mL of acetonitrile was added, in air, just before a TEM was obtained. A drop of this solution was then dispersed on a chloroform cleaned, carbon-coated Cu TEM grid.

TEM samples of subnanometer gold clusters were prepared as previously reported[21a−d]. Purified samples of 2-[2-(2-mercapto-ethoxy)-ethoxy]-ethanol (hereafter mercaptoexthoxyethxoyethanol) stabilized clusters were dissolved in methylene chloride and a few microliters of this solution was aerosoled (from a fine capillary by application of compressed air), onto carbon holey carbon or silicon monoxide films on Cu TEM grids.

Sample TEM Analyses. TEM analyses of samples prepared as described above were performed at the University of Oregon with the expert assistance of Drs. Eric Schabtach and JoAn Hudson on a Philips CM-12 TEM with a 70 μm lens operating at 100 kV and with a 2.0 Å point-to-point resolution, all as described previously in detail[28]. Typically, TEM pictures of each sample were taken at 3 different magnifications (100, 430, and 580 K) in order to obtain information about the sample in general (100 K), plus a closer visualization of the clusters (580 K). A number of control experiments were performed previously (primarily for the $Ir(0)_n$ nanoclusters[21a−d]), which provided good evidence that the results are truly representative of the sample (i.e., save any crystallization of the nanoclusters in the electron beam) and that the sample is not otherwise perturbed by application of the TEM beam [e.g., controls showing that varying the sample aerosoling method (in air or under N_2) or depositing the sample as a drop and letting it dry did not change the results; controls showing that changing the beam voltage from 40 to 100 kV, or changing the exposure time (seconds vs. minutes), did not change the images; other controls have been done as well[27]].

Particle Size Measurements. Particle size analyses were performed using NIH-Image 1.62 (for Mac OS) or Scion Image for Windows (Beta 4.02). The following steps were taken to prepare the data for analysis: (i) a bright field TEM image was obtained with even illumination. Images were chosen to be as representative of the bulk sample as possible; (ii) a photographic negative of the image was then scanned into a computer using a scanning camera (Lumina) or flatbed transparency scanner (1200 dpi, 8-bit grayscale) and saved as a TIFF file; (iii) using Adobe Photoshop^{TM}, the contrast/brightness and channel curves were adjusted so that the particles stand out clearly from the background. This is the most difficult for small particles, which inherently have less contrast. Note that the best results are typically obtained when the image contrast is high and minimal image processing is required. In *Image*, after having set the scale and the threshold (the threshold was set to a uniform value for the whole image), the "Analyze Particles" feature was used to generate a table of particle areas and diameters (output as major and minor axes). This table was then exported into Microsoft Excel, where histograms, statistical analysis, and histogram plotting were performed. For each particle, the diameter was calculated by 1 of 2 ways: from the area by assuming that the nanoclusters are circular (the Ir(0) or Pd(0) nanoclusters, in the work done at CSU) or by taking the average of major and minor axes (the Au(0) nanoclusters, in the work done at Oregon). Size distributions

are quoted as the mean diameter ± the standard deviation.

Results and Discussion

Figure 1 shows a 430 K magnification TEM image, and the associated particle size histogram (367 non-touching particles counted by NIH-Image), of isolated 2.3 ± 0.5 nm $Ir(0)_{\sim 300}$ nanoclusters grown by hydrogen reduction of 1.2 mM $[(1,5\text{-COD})Ir(CH_3CN)_2]BF_4$ with 1.2 mM $[Bu_4N]_3[citrate^{3-}]$ in acetone under the hydrogenation conditions described as "Standard Conditions" elsewhere[25]. This case was chosen as an example of TEM images with a clear background; hence, both setting the threshold and counting the particles are straightforward. All of the non-touching 367 particles could be counted.

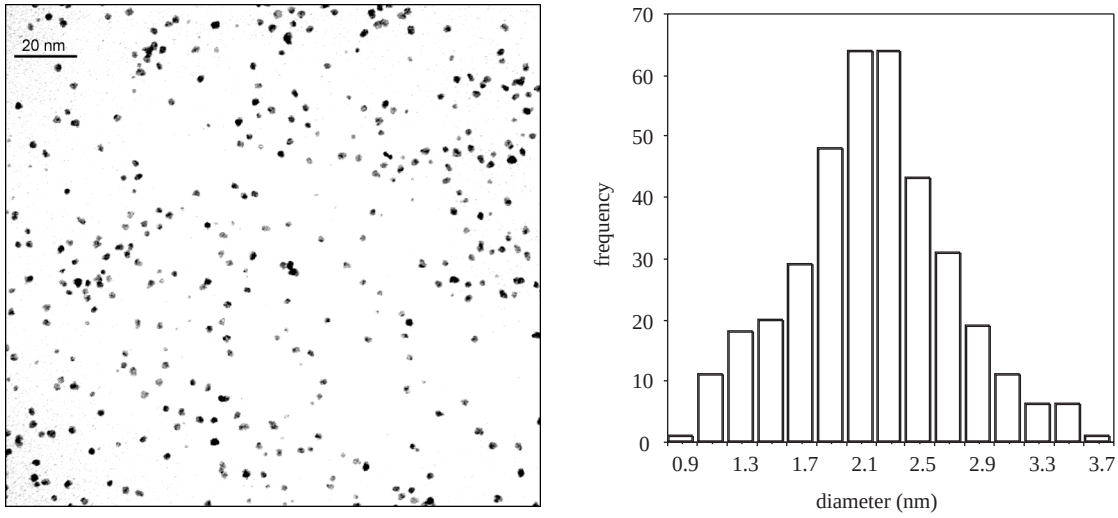

Figure 1. (a) TEM image (430 K magnification) and (b) associated particle size histogram (367 non-touching particles counted by NIH-Image) of isolated 2.3 ± 0.5 nm $Ir(0)_{\sim 300}$ nanoclusters grown by hydrogen reduction of 1.2 mM $[(1,5\text{-COD})Ir(CH_3CN)_2]BF_4$ with 1.2 mM $[Bu_4N]_3[citrate^{3-}]$ in acetone under Standard Conditions at 22.0 ± 0.1 °C and 40 ± 1 psig H_2 as described in the Experimental section elsewhere.[21d] The sample was harvested after 10 h under the hydrogenation conditions detailed elsewhere[21d] since it was clear that bulk metal, due to agglomeration, had already precipitated.

The second example, Figure 2, also gives a well-defined TEM; however, the contrast and background are not as uniform as for the sample in Figure 1. Consequently, setting the threshold to a higher value for the darker portion of the image (i.e., the lower left of Figure 2) or to a lower value for the lighter portion (e.g., the middle or upper right of Figure 2) reduces or increases, respectively, the number of particles counted. Since the number of isolated particles is higher in this example, one can count 405 non-touching particles with only a single threshold value.

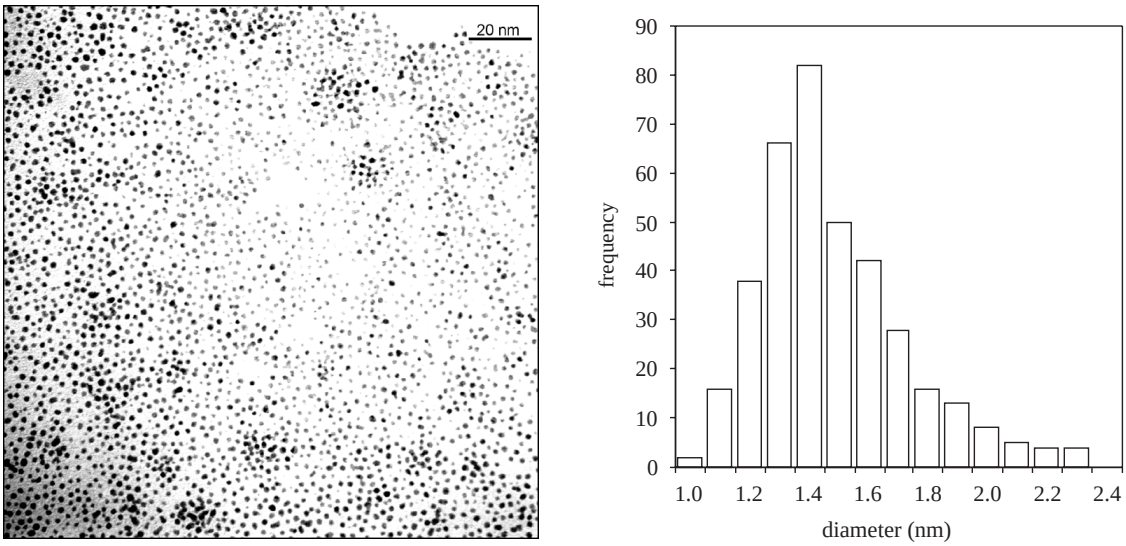

Figure 2. (a) TEM image (430 K magnification) and (b) associated particle size histogram (405 non-touching particles counted by NIH-Image) of isolated 1.5 ± 0.3 nm $Ir(0)_{\sim 300}$ nanoclusters formed from the reduction of 1.2 mM $[Bu_4N]_5Na_3[(1,5\text{-COD})Ir{\cdot}P_2W_{15}Nb_3O_{62}]$ in acetone at 22.0 ± 0.1 °C and 40 ± 1 psig H_2 as described in the Experimental section and "Standard Conditions" available elsewhere.[21d] The sample was harvested after 4 h hydrogenation corresponding to about 60% conversion of the $[(1,5\text{-COD})Ir(I)]^+$ complex to Ir(0) as determined by GLC monitoring of the cyclooctane evolved during the reduction.[21d].

Three additional TEM images of Ir(0) nanoclusters are shown in Figures 3−5, and an image of Pd(0) nanoparticles is shown in Figure 6. In each case, a significant number of non-touching particles could be counted by NIH-Image (490 to 1905 particles). The specific examples in Figures 3-5 were chosen to illustrate the following points: Figure 3, an asymmetric histogram due to the lack of detection of particles smaller than 1 nm in diameter; Figure 4, tailing indicative of particle agglomeration;[29] and Figure 5, a nicely symmetrical distribution made apparent by the ability to count 669 particles using *Image*. Figure 6 illustrates a TEM image of Pd(0) nanoclusters with a larger number of particles. By using NIH-Image 1905 non-touching particles were counted quickly within a few minutes. The resulting histogram suggests a bimodal distribution, one that would be less clear or could have been easily missed in the counting of a smaller number particles by eye / hand. (The statistically appropriate methods for verifying, or refuting, such suspected bimodal distributions in TEM analyses are already available in our prior literature[30] for the interested reader; hence, we need not repeat that information here.)

Figures 7 and 8 show TEM images deliberately chosen to illustrate cases where one has problems counting the nanoclusters with programs such as *Image* given the quality of the image. Indeed, a key concern in the images in Figures 7 and 8 is whether or not it is even appropriate to use *Image*. Or, should one optimize the sample preparation to obtain a "better" image? This latter approach raises, in turn, the key concern of images of non-homogeneous samples: one must avoid reporting selected, "somehow-arbitrarily-determined-to-be-the-best", images of inhomogeneous samples in order to ensure a representative analysis[13].

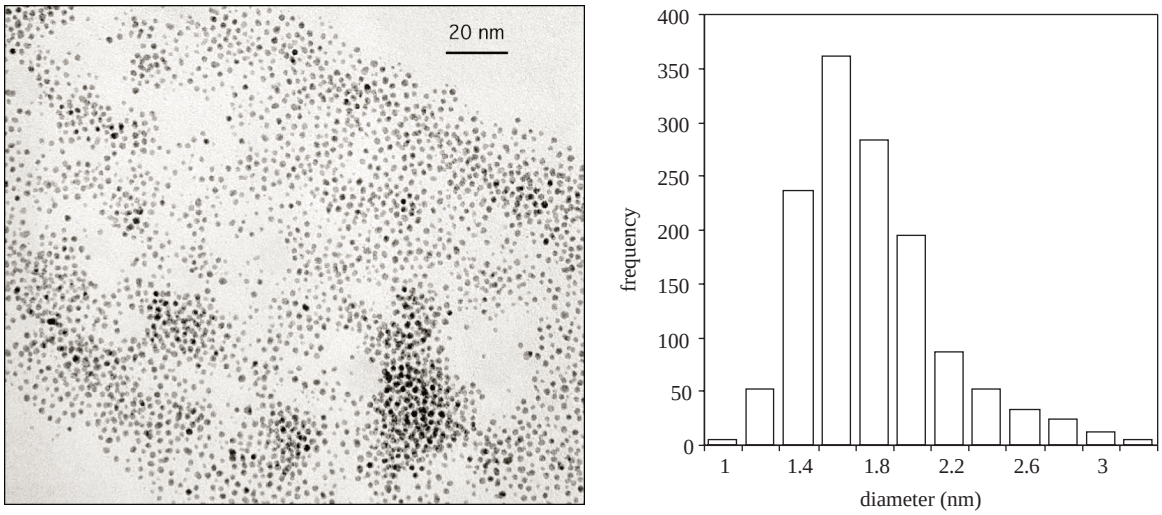

Figure 3. (a) TEM image (430 K magnification) and (b) associated particle size histogram (1490 non-touching particles counted using NIH-Image) of isolated 1.8 ± 0.4 nm Ir(0) nanoclusters grown by the reduction of 1.2 mM $\{(Bu_4N)[(1,5\text{-COD})IrHPO_4]\}_2$ in acetone at 22.0 ± 0.1 °C and 40 ± 1 psig H_2 and harvested after 40 h as described in the Experimental section elsewhere[21c]. Note that the histogram shows some apparent tailing to higher diameters, a result which is very likely due to the non-detection of nanoclusters ≤ 1.0 nm in this case, and not due to nanoparticle agglomeration.

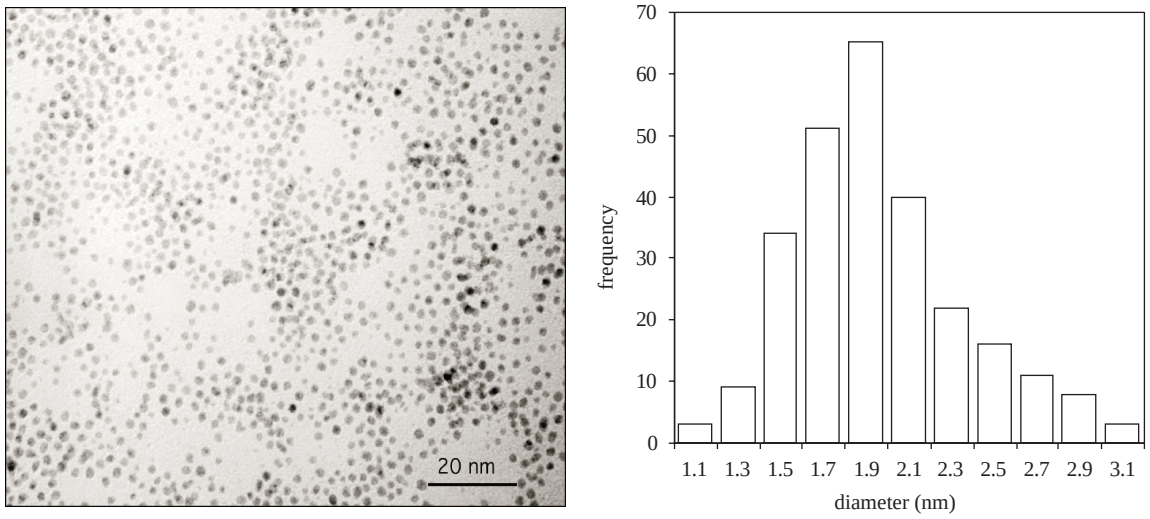

Figure 4. (a) TEM image (580 K magnification) and (b) associated particle size histogram (490 non-touching particles, counted using NIH image) of isolated 1.8 ± 0.4 nm (±22%) Ir(0) nanoclusters grown by the reduction of 1.2 mM $\{(Bu_4N)[(1,5\text{-COD})IrHPO_4]\}_2$ in acetone at 22.0 ± 0.1 °C and 40 ± 1 psig H_2 as described in the Experimental section elsewhere[21c]. The sample was harvested after 40 h reaction at which point a cyclooctane evolution by GLC showed the nanocluster formation was complete. The noticeable tailing in the histogram is indicative of some nanocluster agglomeration.

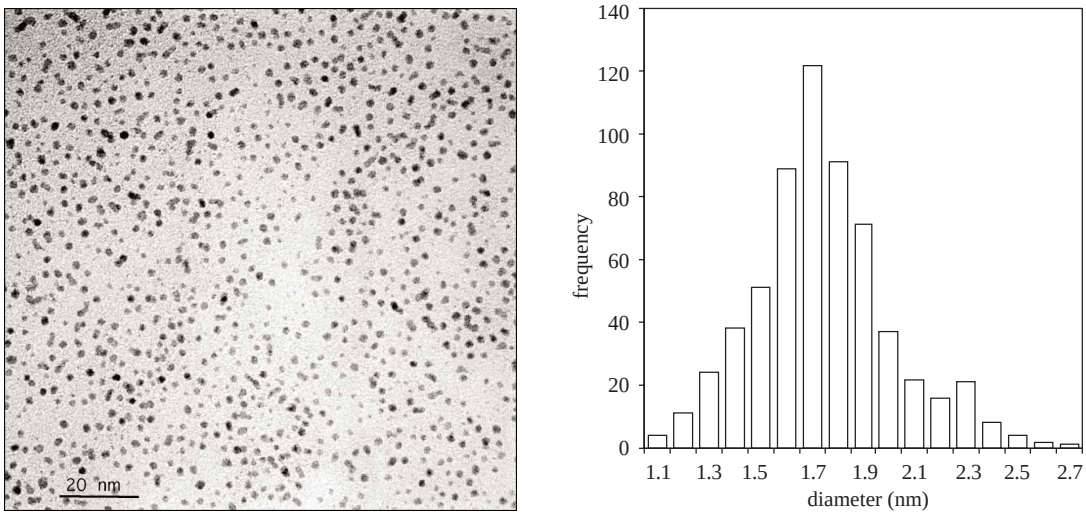

Figure 5. (a) TEM image (580 K magnification) and (b) associated particle size histogram (669 non-touching particles counted using NIH-Image) of isolated, 1.8 ± 0.4 nm Ir(0) nanoclusters grown by the reduction of 1.2 mM $\{(Bu_4N)[(1,5\text{-COD})IrHPO_4]\}_2$ and 1.2 mM Proton Sponge^{TM} in acetone at 22.0 ± 0.1 °C and 40 ± 1 psig H_2 as described in the Experimental section elsewhere.[21c] The sample was harvested after 14 h reaction (i.e., the nanoclusters are deliberately not fully formed) since we wished to examine the nanocluster distribution before any agglomeration [26] became more pronounced. The nicely symmetric distribution is noteworthy.

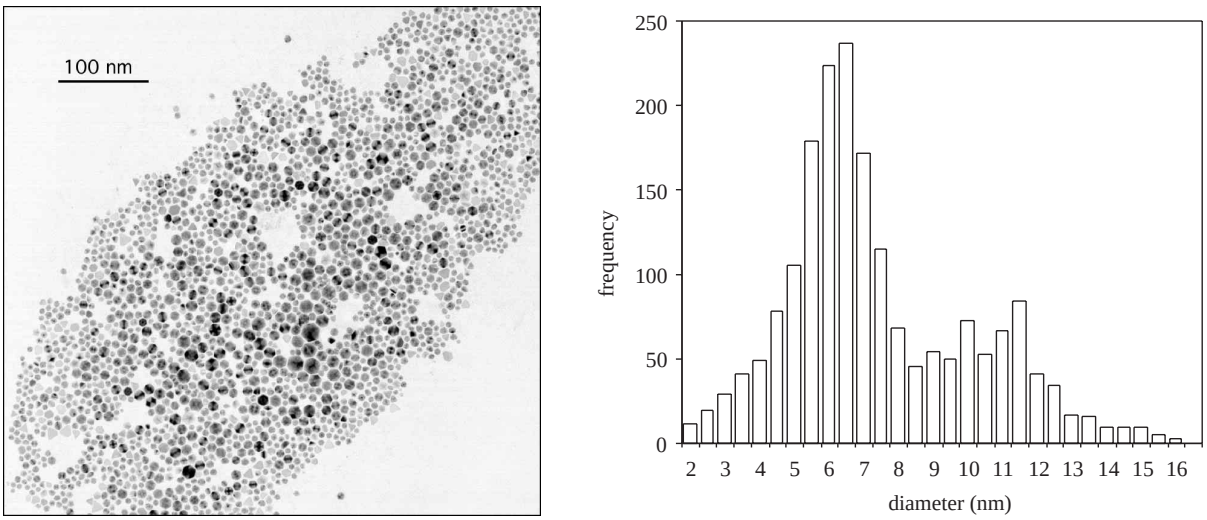

Figure 6. (a) TEM image (100 K magnification) and (b) associated histogram (1905 non-touching particles counted by NIH-Image) of palladium(0) nanoclusters formed from the reduction of $[Pd(acac)_2]$ during cyclohexene hydrogenation in propylene carbonate at 22 ± 0.1 °C in the presence of 1 equivalent $[Bu_4N]_2HPO_4$.[21d] The sample was harvested after 8 h.

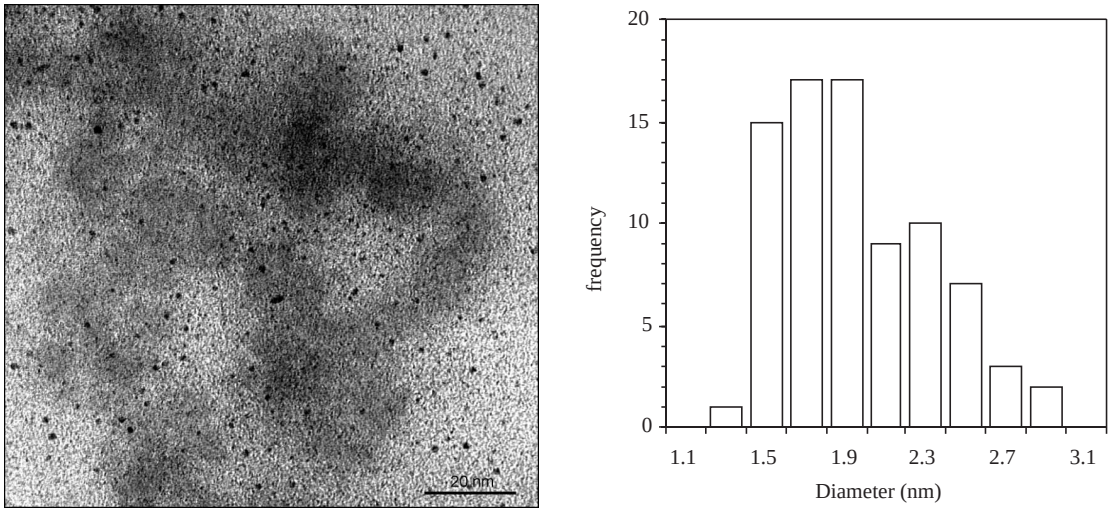

Figure 7. (a) TEM images (430 K magnification) and (b) associated histogram of Ir(0) nanoclusters formed from 0.72 μmol $\{(Bu_4N)[(1,5\text{-COD})IrHPO_4]\}_2$ and 0.72 μmol (1 equivalent) of Proton Sponge^{TM} after a cyclohexene hydrogenation catalytic lifetime experiment involving 150,000 total turnovers of cyclohexene hydrogenation by the nanoclusters at 22 $\pm$ 0.1 ^{o}C and 40 $\pm$ 1 psig H_2 as detailed elsewhere.[21c] The nanoclusters were isolated after completion of the total turnovers experiment, then redissolved in acetonitrile and placed on a TEM grid. The bottom TEM and associated histogram show 19 $\pm$ 5 Å particles (only n = 81 non-touching particles could be counted).

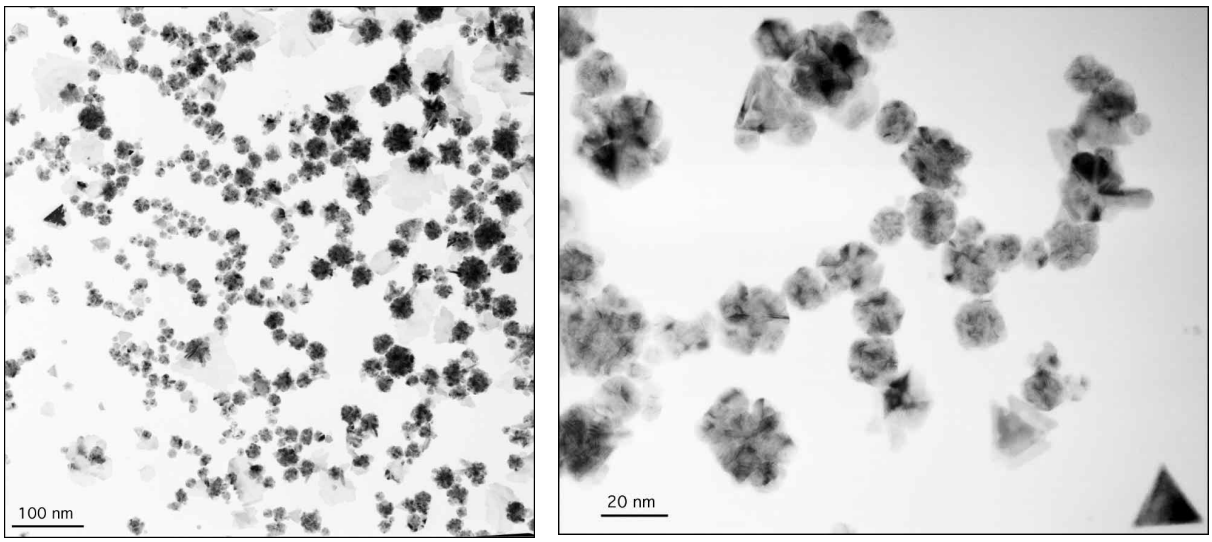

Figure 8. (a) 100 K and (b) 430 K magnification TEM images of aggregated palladium(0) nanoclusters formed from the reduction, under 1 atm of hydrogen, of $[Pd(acac)_2]$ in propylene carbonate at 22 $\pm$ 0.1 °C[21d].

Figure 7 illustrates a case where the particles are not readily recognizable due to the presence of a darker background (due, in turn, probably to the formation of bulk Ir(0) metal in those sections). In this case, the contrast and darkness of the separate sections of the TEM picture were adjusted in Adobe Photoshop^{TM} prior to the analyzing of particles by NIH-Image. Even so, only a small number (81) of particles could be counted. Controls were done to show that the choice of sections did not influence the results significantly; a

key here is to be sure that changing the threshold setting does not change the area of the particles measured. Additional controls showed that 3 NIH-Image analyses, performed by using randomly selected sections, plus 1 visual analysis of the particles, gave size distributions very similar to the one given in Figure 6 (i.e., experimentally 1.9 ± 0.2 nm; the resolution of the instrument is ±0.2 nm, and so the true error bars here are more like ±0.5 nm in our experience).

Figure 8 shows a TEM micrograph of Pd(0) nanoclusters, where almost all of the particles stick together as one can see better in the right-hand picture taken with 430 K magnification. In such cases, reliable particle counting is impossible with or without touching particles being ignored. This is not due to any inherent inability of *Image*; instead, it is due to either the poor nature of the sample preparation or the inherent tendency of the nanoparticles to aggregate (or both). Attempting to obtain reliable particle size statistics from this TEM image, using either *Image* or via a tedious visual inspection, is inviting misinterpretation.

As a final example of the utility of the *Image* program, the analysis of images of 0.8 nm (core diameter) gold particles is given in Figure 9. The difficulties of computer-assisted analyses of images of sub-1-nm particles have been noted[14]. However, by taking appropriate care in sample preparation, microscopy and image analysis, we show below that large populations of subnanometer particles can be analyzed readily and precisely. First, the use of holey carbon-coated grids is needed to reduce the graininess of the image background, making it easier to distinguish small clusters from the grid background and measure them. Further, aerosol deposition (as opposed to dip- or drop-casting) of the sample onto the grid has been employed in the micrographs in Figure 9 to reduce or eliminate aggregation, thereby simplifying the data analysis with *Image*. (In a number of cases we have found superior results using aerosol deposition.) Of course, appropriate alignment of the electron beam, precise astigmatism correction and correct exposure of the negative to ensure even illumination are prerequisites to producing high-quality negatives for analysis[13c]. In Figure 9b, the gold particles were aerosoled onto a holey carbon-coated TEM grid. The particles are clearly distinguished from any grain in the supporting film and very few aggregates are present. Using this approach and *Image* for analysis, measurement of hundreds of subnanometer particles is straightforward: 358 particles were counted to obtain a size of 0.8 ± 0.3 nm. In contrast, the micrograph in Figure 9a was obtained by aerosoling a sample of the same gold nanoparticles onto a regular carbon-coated TEM grid. Here, the graininess of the support film leads to a significant increase in artifacts that are being counted as apparent particles. This clearly changes the overall average "particle" size and size distribution as the histogram provided in Figure 9a reveals, resulting in incorrect results. In this case, 960 "particles" are counted to obtain an artificially small size of 0.6 ± 0.3 nm.

Strategies and caveats when using image

Image—like TEM itself—is most useful in analyzing images exhibiting high, uniform contrast of isolated particles. As emphasized earlier in this paper, an appropriate choice of grids, sample deposition techniques and TEM imaging conditions are keys to obtaining excellent images for analysis. The problem in particle boundry vs. grid contrast is always likely to be the major issue to be overcome. The "ignoring touching particles" option in *Image* will reduce the number of particles counted and will underemphasize the larger particles; hence, this option should be used with caution and, instead, attempts at preparing a better dispersed sample by, for example, aerosol deposition should be tried. In cases exhibiting non-uniform contrast (e.g., darker sections), dividing the TEM image into sections with different contrast can be done.

However, one has to be aware of the caveat that setting the threshold value too low or too high might lead to elimination of small particles or creation of imaginary, non-real, small particles, respectively. Controls can and should be done, as were done herein, to see whether or not the choice of the sections significantly influences the results.

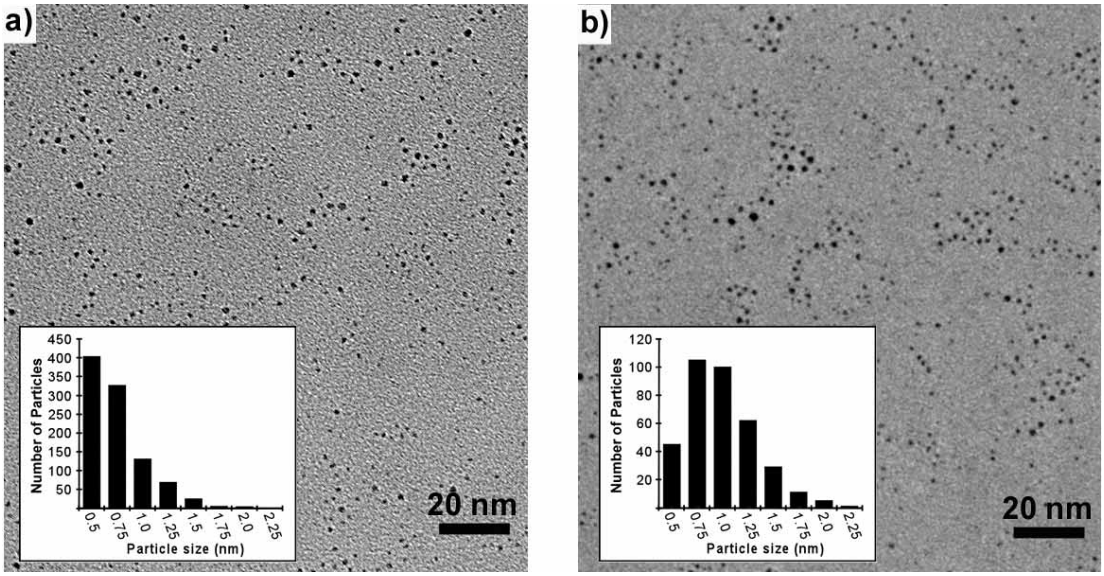

Figure 9. TEM images (430 K magnification) of mercaptoexthoxyethxoyethanol-stabilized Au nanoclusters (0.8 ± 0.3 nm) aerosoled onto (a) traditional carbon-, and (b) holey carbon-coated grids. Note that the much less grainy background in the micrograph obtained using the holey carbon-coated grids, Figure 9b, allows the sub-1-nm particles to be imaged and counted accurately.

Another challenge arises when nanoparticles of different shape are present. *Image* measures the area of the particle images (based upon the number of pixels comprising the particle) and the shortest (minor) and longest (major) axes of each particle. For the cases described in this paper, the core size is obtained from the area measured assuming the particles are spherical (i.e., a circular 2 dimensional image) or by taking the average of the major and minor axes. Either of these approaches works well for spherical particles. However, there are a number of examples of non-spherical particles, for example, El-Sayed's platinum nanoclusters, where tetrahedral, cubic and truncated octahedral particles are present[31]. We have not explored the use of *Image* for such cases, but we expect it to prove less useful for such more complicated systems containing multiple nanoparticles of different shapes within the same sample grid.

Next, a more general caution is in order concerning the computer-aided reconstructing of TEM images. It is essential to compare each reconstructed image (after digital processing and analysis by *Image*) to the original to ensure that the size and shape of the particles are preserved. For example, compare Figure 2a and 2b on p. 8781 elsewhere[14] the apparent difference between the real (2a) and manipulated (2b) pictures reveals that the middle portion is the most populated area in the real image, but has almost no particles in the manipulated image. In our own work, we often compare computer overlays or overlays using overhead transparencies to compare reconstructed images to the originals. In short, one needs to exercise extreme caution during digital image manipulations—is one counting all the particles and only particles?

Finally, *Image* is of course not a solution to the underlying problems of TEM as a method of semi-quantitative particle-size measurements[13c]; *Image* is also not a solution to the problems of TEM in visualizing

lower contrast materials such as Co, Fe or Ni (first-row transition metal) nanoclusters or, for example, $(ZnS)_n$, $(Si)_n$ or other, lighter atom nanoparticles. In addition, no claim is made that this paper covers all the issues that are worthy of further investigation: one is the need to compare HR-TEM counting of lattice fringes to obain particle sizes, followed by comparing and contrasting those results to the results from *Image* as well as the results from small angle X-ray or other light-scattering methods on the same, identical sample. Instead, the present contribution's main intent is to point out that there is no longer an excuse for not counting a statistically useful numbers of particles.

In summary, *Image* is a free, public-domain program that is useful for the rapid counting of statistically valid numbers of particles in TEM images in which good contract TEM data is available, and when attention is paid to the caveats and suggestions for its appropriate use.

Acknowledgments

Support for the work at Colorado State University was provided by the Department of Energy, Office of Basic Energy Sciences, via DOE grant FG06-089ER13998, and for the work at the University of Oregon by the National Science Foundation (DMR-9705343).

References

1. Reviews: (a) G. Schmid, M. Baumle, M. Geerkens, I. Heim, C. Osemann and T. Sawitowski, Chem. Soc. Rev. 28, 179-185 (1999). (b) G. Schmid and L.F. Chi, Adv. Mater. 10, 515-518 (1998). (c) J.H. Fendler, "**Nanoparticles and Nanostructured Films**". Weinheim, Wiley-VCH, 1998. (d) A. Fürstner, "**Active Metals: Preparation, Characterization, and Applications**". Weinheim: VCH, 1996. (e) J.S. Bradley, "The Chemistry of Transition Metal Colloids". In G. Schmid, editor. Clusters and Colloids. From Theory to Applications, pp. 459-544, New York, VCH, 1994. (f) G. Schmid, **Chem. Rev. 92**, 1709-1727 (1992). (g) An excellent series of papers, including a record of the insightful comments by the experts attending the conference, is available in: **Faraday Discussions 92**, 1-300 (1991).
(h) G. Schmid, "**Large Transition Metal Clusters-Bridges Between Homogenous and Hetereogenous Catalysts"**. In R. Ugo, editor. Aspects of homogeneous catalysis. Chapter 1, Dordrecht: Kluwer, 1990. (i) R.P. Andres, R.S. Averback, W.L. Brown, L.E. Brus, W.A. III Goddard, A. Kaldor, S.G. Louie, M. Moscovits, P.S. Peercy, S.J. Riley, R.W. Siegel, F. Spaepen and Y.J. Wang, **J Mater. Res. 4**, 704-736 (1989). (j) A. Henglein, **Chem. Rev. 89**, 1861-1873 (1989). (k) J. M. Thomas, **Pure Appl. Chem. 60**, 1517-1528 (1988). (l) P. Jena, B.K. Rao and S.N. Khanna "**Physics and Chemistry of Small Clusters"**. New York, Plenum, 1987.

2. (a) J.D. Aiken III and R.G. Finke, **J. Mol. Cat. A Chem. 145**, 1-44 (1999).
(b) J.D. Aiken III, Y. Lin and R.G. Finke, **J. Mol. Cat. A Chem. 114**, 29-51 (1996). (c) R. G. Finke, "**Transition metal nanoclusers- Solution phase synthesis, then characterization and mechanism of formation, of polyoxoanion- and tetrabutylammonium-stabilized nanoclusters"** in D.L. Feldheim and C.A. Foss Jr., editors. Metal Nanoparticles: Synthesis, Characterization and Applications. pp. 17-54, New York, Marcel Dekker, 2002.

3. (a) R. Turton, "**The Quantum Dot: A Journey into the Future of Microelectronics**". New York, Oxford University Press, 1995. (b) H. Haberland, "**Clusters of atoms and molecules**", New York, Springer-Verlag, 1994.

4. (a) G. Schmid, "**Clusters and Colloids; From Theory to Applications**". New York: VCH Publishers, 1994. (b) L.J. de Jongh, "**Physics and Chemistry of Metal Cluster Compounds**", Dordrecht, Kluwer Publishers, 1994.
5. (a) J. Stein, L.N. Lewis, Y. Gao and R.A. Scott, **J. Am. Chem. Soc. 121**, 3693- 3703 (1999). (b) M.T. Reetz, R. Breinbauer, P. Wedemann and P. Binger, **Tetrahedron 54**, 1223-1240 (1998). (c) T.J. Schmidt, M. Noeske, H.A. Gasteiger, R.J. Behm, P. Britz, W. Brijoux and H. Bönnemann, **Langmuir 13**, 2591-2595 (1997). (d) G. Schmid, V. Maihack, F. Lantermann and S. Peschel, **J. Chem .Soc. Dalton Trans**. 589-595 (1996). (e) M.T. Reetz and G. Lohmer, **Chem. Commun**., 1921-1922 (1996). (f) M.T. Reetz, R. Breinbauer and K. Wanninger, **Tetrahedron Lett. 37**, 4499-4502 (1996). (g) M.T. Reetz, S.A. Quaiser, and C. Merk, **Chem. Ber. 129**, 741-743 (1996). (h) H. Bönnemann and G.A. Braun, **Angew. Chem. Int. Ed. Eng. 35**, 1992-95 (1996). (i) L.N. Lewis, **Chem. Rev. 93**, 2693-2730 (1993). (j) M.N. Vargaftik, V.P. Zargorodnikov, I.P. Stolarov, I.I. Moiseev, D.I. Kochubey, V.A. Likholobov, A.L. Chuvilin and K.I. Zamaraev, **J. Mol. Cat. 53**, 315-348 (1989).
6. J. Glanz, **Science 269**, 1363-1364 (1995).
7. (a) G. Schön and U. Simon, **Coll. Poly. Sci. 273**, 202-218 (1995). (b) M. Antonietti and C. Göltner, **Angew. Chem. Int. Ed. Eng. 36**, 910-28 (1997). (c) V.L. Colvin, M.C. Schlamp and A.P. Alivisatos, **Nature 370**, 354-357 (1994).
8. R. Elghanian, J.J. Storhoff, R.C. Mucic, R.L. Letsinger and C.A. Mirkin, **Science 277**, 1078-1081 (1997).
9. S.V. Sonti and A. Bose, **J. Colloid Int. Sci. 170**, 575-585 (1995).
10. M.T. Reetz, M. Winter, G. Dumpich, J. Lohau and S. Friedrichowski, **J. Am. Chem. Soc. 119**, 4539-40 (1997).
11. T. Vossmeyer, E. DeIonno and J.R. Heath, **Angew. Chem. Int. Ed. Eng. 36**, 1080-83 (1997).
12. (a) B.V. Miller and R.W. Lines, **CRC Crit. Rev. Anal. Chem**. **20**, 75-116 (1988). (b) T.N. Baker, **Microstructure of High Temperature Materials 5**, 161-189 (2001).
13. (a) Obtaining a truly representative group of images of the sample at hand[b] is, as is well known[c], the necessary first step of using correctly TEM and other powerful, atomic-level microscopies. First, the sample needs to be as homogeneous to the eye and to lower power microscopies; the presence of multilayered samples or precipitates, for example bulk metal, virtually assures problems in obtaining representative micrographs in our experience. Next, a group of 10-20 randomly selected TEM micrographs at lower power (for example $\leq$100 K magnification) needs to be obtained, followed by any needed higher magnification micrographs. Restated, the particle counting software and resultant statistics used herein rely, of course, on one first obtaining truly representative micrographs of the system being examined;
    (b) The problem of obtaining a truly representative set of micrographs is what we like to call the "Avogadro's Number Problem" to remind us how far away, from an Avogadro's number collection of particles, the sample size being examined by TEM actually is.
    (c) Transmission electron microscopy books: D.B. Williams and C.B. Carter, "**Transmission electron microscopy: a textbook for materials science"**. New York, Plenum Press, 1996. M.A. Hayat, "**Basic techniques for transmission electron microscopy**", Orlando, Academic Press, 1986. L. Reimer, "**Transmission electron microscopy: physics of image formation and microanalysis**", Third Edition, New York, Springer-Verlag, 1993. A.C. McLaren, "Transmission electron microscopy of minerals and rocks", Cambridge, Cambridge University Press, 1991.
14. M.T. Reetz, M. Maase, T. Schilling and B. Tesche, **J. Phys. Chem. B 104**, 8779-8781 (2000).

15. MACS (Measurements and Automatic Counting Software, which runs on a Unix worksation): J.-P. Rolland, P. Bon and D. Thomas, **Computer Applications in the Biosciences 13**, 563-64 (1997).

16. R. Fisker, J.M. Carstensen, M.F. Hansen, F. Bodker and S. Morup, **J. Nanoparticle Research 2**, 267-277 (2000).

17. SPIP: The Scanning Probe Image Processor, from Image Metrology ApS, Denmark. http://www.imagemet.com/spip/spip.html.

18. LUCIA: Laboratory Universal Computer Image Analysis, from Laboratory Imaging, Czech Republic. (a) I. Srnova-Sloufova, F. Lednicky, A. Gemperle and J. Gemperlove, **Langmuir 16**, 9928-35 (2000). (b) J. Kaasova, P. Kadlec, Z. Bubnik, J. Prihoda, **Czech J. Food Sci. 18**, 249-250 (2000).

19. KONTRON KS 400: from Zeiss-Kontron, Germany. (a) L. Connolly, P. Maxwell, **British J. Biomed. Sci. 59**, 11-14 (2002). (b) M. Quinten, A. Heilmann and A. Kiesow, **Appl. Phys. B 68**, 707-712 (1999).

20. Scion Image 1.63 is a free modification of the NIH-Image 1.63 by Scion Corporation (Frederick, MD: http://www.scioncorp.com). The download page is: http://www.scioncorp.com:8080/Downloads/fr_login.htm. Current versions are Scion Image 1.63 for MacOS 7.5 to 9.x and Scion Image Beta 4.02 for Windows 95, 98, ME, NT 2000 and XP.

21. (a) S. Özkar and R. G. Finke, **J. Am. Chem. Soc. 127**, 4800-08 (2005). (b) S. Özkar and R. G. Finke, **Langmuir 19**, 6247-60 (2003). (c) S. Özkar and R. G. Finke, **Langmuir 18**, 7653-62 (2002). (d) S. Özkar and R. G. Finke, **J. Am. Chem. Soc. 127**, 5796-5810 (2002). (e) S. Ichinose, T. Muneta, H. Aoki and M. Tagami, **Biomed. Mater. Engin. 13**, 125-34 (2003).

22. One of us (J.E.H.) initiated our use of this program as briefly reported elsewhere: (a) L.O. Brown and J.E. Hutchison, **J. Phys. Chem. B 105**, 8911-16 (2001). (b) W.W. Weare, S.M. Reed, M.G. Warner and J.E. Hutchison, **J. Am. Chem. Soc. 122**, 12890-91 (2000). (c) M.G. Warner, S.M. Reed and J.E. Hutchison, **Chem. Mater. 12**, 3316-20 (2000). (d) L.O. Brown and J.E. Hutchison, **J. Am. Chem. Soc. 121**, 882-883 (1999). (e) L.O. Brown, J.E. Hutchison, **J. Am. Chem. Soc. 119**, 12384-85 (1997).

23. Literature suggesting that smaller, often undetected Au nanoparticles under 1-2 nm are present in at least some literature syntheses of Au nanoparticles: (a) P. Riello, P. Canton and A. Benedetti, Langmuir 14, 6617-19 (1998). (b) J.P. Wilcoxon and S.A. Craft **Nanostructured Materials 9**, 85-88 (1997).
(c) J. P. Wilcoxon, J. E. Martin, P. Provencio, **Langmuir 16**, 9912-20 (2000).

24. Cases where undetected, subnanometer Au nanoclusters, present in addition to larger Au nanoclusters, may be involved in the observed chemistry: (a) L.H. Lu, H.S. Wang, S.Q. Xi and H.J. Zhang, **J. Mater. Chem. 12**, 156-158 (2002). (b) N. R. Jana, L. Gearheart and C.J. Murphy, **Chem. Mater. 13**, 2313-22 (2001).

25. S. Özkar and R.G. Finke, manuscript in preparation, (Palladium(0) nanoclusters catalysts)

26. G.H. Woehrle, M.G. Warner and J.E. Hutchison, **J. Phys. Chem. B 106**, 9979-9981 (2002).

27. Y. Lin and R.G. Finke, **J. Am. Chem. Soc. 116**, 8335-8353 (1994).

28. Y. Lin and R.G. Finke, **Inorg. Chem. 33,** 4891 (1994).

29. B.J. Hornstein and R.G. Finke, Chem. Mater. 16, 139-150 (2004).

30. J.D. Aiken and R.G. Finke, **J. Am. Chem. Soc. 120**, 9545-54 (1998).

31. J.M. Petroski, Z.L. Wang, T.C. Green and M.A. El-Sayed, **J. Phys. Chem. 102**, 3316-20 (1998).